This article has been accepted for inclusion in a future issue of this journal. Content is final as presented, with the exception of pagination.

Finite Horizon Nonlinear Energy Optimizing Control in a Force Augmenting Hybrid Exoskeleton for the Elbow Joint

Fermín Castillo, Ricardo López-Gutíerrez, Omar-Jacobo Santos-Sánchez, Antonio Osorio, Sergio Salazar, and Rogelio Lozano,

***Abstract*— In this brief, the implementation of a suboptimal nonlinear discrete control to optimize the energy consumption in a hybrid exoskeleton for the elbow joint is presented. The exoskeleton is used to amplify the strength of the user and is hybrid in the sense that it combines two types of actuators: pneumatic muscles and Harmonic Drive motors, which give power and precision to the system, respectively. The exoskeleton is autonomous in the energetic sense, and it is driven by compressed air and batteries. The suboptimal control is used to increase the operation time of the exoskeleton. This control law penalizes the energy consumption, and it has a direct effect on the operation time of the prototype.**

***Index Terms*— Force increment, hybrid exoskeleton, suboptimal control.**

I. Introduction

TECHNOLOGICAL progress in exoskeletons has considerably grown in recent years, and thanks to this fact, mankind enjoys a comfortable life. One of the research areas being explored to improve quality life is the exoskeleton robots. Scientific and technological work in exoskeletons dates back to the early 1960s. "The exoskeleton is a kind of wearable robot. The distinctive, specific, and singular aspect of exoskeletons is that the exoskeleton kinematic chain maps on to the human limb anatomy. There is a one-to-one correspondence between human anatomical joints and the robot joints or sets of joints" [1].

Some exoskeletons employ pneumatic muscles as main actuators that generate the desired movement of a determined joint of the body. Ramos *et al.* [2] proposed an exoskeleton that uses pneumatic actuators to amplify the strength of a superior limb, and the prototype is controlled by electromyography (EMG) signals and presents experimental results.

Noda *et al.* [3] worked on an exoskeleton using pneumatic muscles in an antagonistic manner transmitting force by a cable and also included two small electromagnetic motors, with a small but effective force amplification. Pujana-Arrese *et al.* [4] presented a 1-DOF control system using pneumatic muscles. The muscles were designed and built for performing research in the industry. The experimental configuration is very nonlinear and very difficult to control. These approaches use pneumatic muscles in different configurations and are controlled employing various control techniques. Putting together pneumatic muscles with some other actuator like electric motor results in a system that takes advantage of the power of the muscles and of the precision or smoothness of the motors. Martinez *et al.* [5] carried out a design of a hybrid exoskeleton, proposing control that has been tested in experiments.

A mathematical model proposed by Pujana-Arrese *et al.* [6] describes the artificial pneumatic muscles and also shows experimental tests when using these actuators. Hamaya *et al.* [7] propose an exoskeleton for superior members and formulate a learning problem to perform a user–robot interface.

Some other exoskeletons are force augmenting devices that employ electrical motors or passive elements as principal actuators to perform a given task. At the 14th International Conference on Ubiquitous Robots and Ambient Intelligence, Seo *et al.* [8] presented the design of an exoskeleton of superior members having 3-DOF with experimental results and new control methods. Sui *et al.* [9] proposed an exoskeleton of 5-DOF for daily living. Liu *et al.* [10] performed a control based on EMG signals for an exoskeleton of upper limbs. The experimental platform of a shoulder and elbow exoskeleton proposed by Crea *et al.* [11] uses elastic actuators in series and has 4-DOF. The exoskeleton proposed by Popov *et al.* [12], [13] is for bidirectional elbow braided on braided rope actuators and proposed a control for this type of actuators.

In some cases, a graphical interface is implemented in the LabVIEW software, where the behavior of the robot or the exoskeleton is depicted in a visual manner. For example, Gou *et al.* [14] performed a control system based on LabVIEW for the upper extremity. Krasin *et al.* [15] presented an exoskeleton of force amplification for the articulation of the elbow, controlled by EMG signals, and the control is programmed through the LabVIEW platform. The work by Cansalar *et al.* [16] presents different simulations of the P, PI, and proportional–integral–differential

Manuscript received June 20, 2019; accepted September 12, 2019. Manuscript received in final form September 27, 2019. This work was supported in part by the French-Mexican Laboratory on Computer Science and Control, International Research Unit, (UMI LAFMIA 3175 CNRS-CINVESTAV) and in part by National Council for Science and Technology (CONACYT). Recommended by Associate Editor G. Rovithakis. *(Corresponding author: Ricardo López-Gutíerrez.)*

F. Castillo, A. Osorio, and S. Salazar are with the French-Mexican Laboratory on Computer Science and Control, Mexico 07360, Mexico (e-mail: fer_castillo3103@hotmail.com; aosorio@cinvestav.mx; sergio.salazar.cruz@gmail.com).

R. López-Gutíerrez is with the National Council for Science and Technology, CONACYT-CINVESTAV, Mexico 07360, Mexico (e-mail: jesusl.lopez@cinvestav.mx).

O.-J. Santos-Sánchez is with the Research Center in Information Technology and Systems "CITIS-ICBI," Autonomous University of the State of Hidalgo, Pachuca 42184, Mexico (e-mail: omarsantos@hotmail.com).

R. Lozano is with the Heuristique et Diagnostic des Systmes Complexes, UMR CNRS 7253, 60200 Compiègne, France (e-mail:rogelio.lozano@hds.utc.fr).

Color versions of one or more of the figures in this article are available online at http://ieeexplore.ieee.org.

Digital Object Identifier 10.1109/TCST.2019.2945021

1063-6536 © 2019 IEEE. Personal use is permitted, but republication/redistribution requires IEEE permission.
See http://www.ieee.org/publications_standards/publications/rights/index.html for more information.

This article has been accepted for inclusion in a future issue of this journal. Content is final as presented, with the exception of pagination.

(PID) controls in the MATLAB/Simulink and LabVIEW platforms. Therefore, the LabVIEW software provides some advantages to implement control loops, such as relative easiness, to implement high-quality graphic interface and capabilities to implement advanced control when is combined with data acquisition instruments. In addition, this software has application in the industry.

Other exoskeletons are designed to rehabilitate joints such as the elbow or shoulder, and their design and control are different.

Gao *et al.* [17] designed an exoskeleton of 3-DOF for the rehabilitation of superior members. Vitiello *et al.* [18] proposed an exoskeleton with a motor in the elbow for physical rehabilitation and the feasibility of the control strategy, and the full system was demonstrated by experimental tests. Mohammad *et al.* [19] presented a rehabilitation exoskeleton for elbow, which includes the movement of the forearm and the wrist at the same time, and the control algorithm tested was a PID control.

One crucial aspect for the exoskeletons is the control strategy used to regulate the desired position and velocity given by the exoskeleton user. However, this aspect is a nontrivial task and it constitutes a challenge due to the system nonlinearities. One requirement mentioned in [20] is to reduce power consumption in the exoskeleton robot, which can be obtained by the development of optimal controllers for portable devices [21]. Nevertheless, the optimal control algorithm synthesis for exoskeletons robots is not an easy task, and its application to this type of prototypes has not yet been done. Indeed, one can cite [22], where the control problem of a hybrid actuation system composed of more than two different types of actuators was addressed, using an discrete dynamic programming (DP) approach; the torque distribution strategy for hybrid actuators was found; a linearization around a specific operation zone was used to find a linear quadratic regulator that was iteratively improved by using of the iterative linear quadratic Gaussian (ILQG) method, and simulation results were presented. In [23], an optimal control framework for the pneumatic artificial muscle (PAM) as a part of the pneumatic-electric (PE) hybrid actuation system was exposed. The model was decomposed into a linear and a nonlinear part, and ILQG was used in order to improve the control law and obtain satisfactory experimental results.

The control law of a hybrid exoskeleton is based on a discrete suboptimal nonlinear algorithm whose purpose is to optimize energy. The consumption of a suboptimal nonlinear discrete control law is used with the aim of extending the autonomy of the exoskeleton and optimization of energy consumption.

The main novelty of this brief is to design and construct an exoskeleton that contains in each elbow joint two types of actuators (two pneumatic muscles and an electric motor) and the control law implementation for each actuator. A joystick placed in the exoskeleton at the height of the user's hand is used to interpret the human intention to flex and extend the elbow joint. The antagonist system formed by pneumatic muscles has been chosen due to the necessary force to move heavy loads.

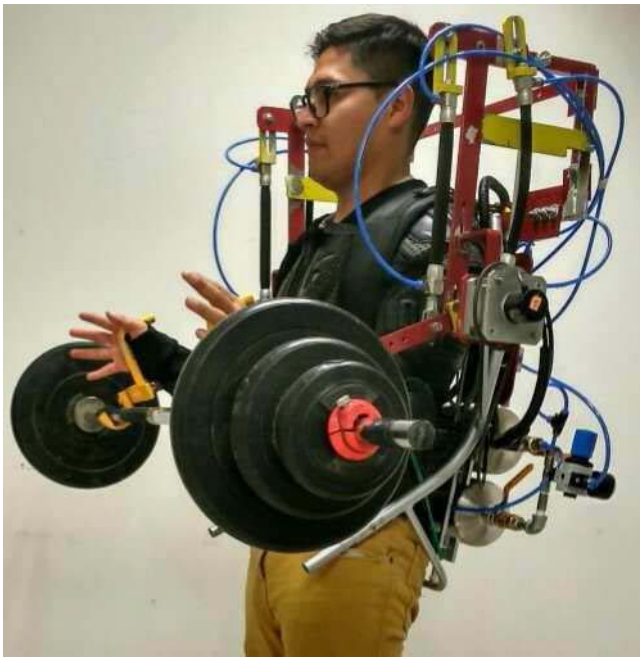

Fig. 1. Force augmenting hybrid exoskeleton for the elbow joints.

TABLE I

EFFORT ANALYSIS, SECURITY FACTOR, ELASTIC LIMIT, DEFORMATION, AND DISPLACEMENT.

Type of Analysis	***Forearm***	***Arm***	***Shoulder***
Security Factor	1.7	20	2.080
Elastic Limit	0.555 N/m^2	1.001 N/m^2	2.003 N/m^2
Deformation	0.001 mm	0.003 mm	0.002 mm
Displacement	0.002 mm	0.001 mm	0.005 mm

High-frequency pneumatic valves were employed to control the air flux entering the pneumatic muscles. However, these components are highly nonlinear and are difficult to control. To overcome this problem, Harmonic Drive electrical motors were employed to give the whole device precision in the last part of the motion of the elbow joint and a nonlinear discrete suboptimal control based on the DP. A discrete nonlinear model of the exoskeleton is considered to design the proposed control algorithm. Note that, for the nonlinear continuous and discrete systems, the synthesis of the optimal controllers is an open problem in control theory, because the function that satisfies the Bellman equation is unknown, so, in this proposal brief, a suboptimal nonlinear discrete sequence is presented, which avoid the solving of the Bellman equation, but in each step, a minimization procedure is executed, which guarantees the achievement of the local minimal. Numerical simulations results have been presented in [24].

II. HYBRID EXOSKELETON DESIGN

A. Mechanical Structure

The complete exoskeleton weighs 7 kg and was designed to have a load capacity of 25 kg. The structure design comprises the dorsal trunk, the shoulder, the arm, the forearm, and the hand, as it is shown in Fig. 1. It is adjustable for people with backs measuring from 40 to 60 cm wide.

The material used in the exoskeleton is 6061-T4 (SS) aluminum and weighs 2.8 kg. A static analysis was performed on

This article has been accepted for inclusion in a future issue of this journal. Content is final as presented, with the exception of pagination.

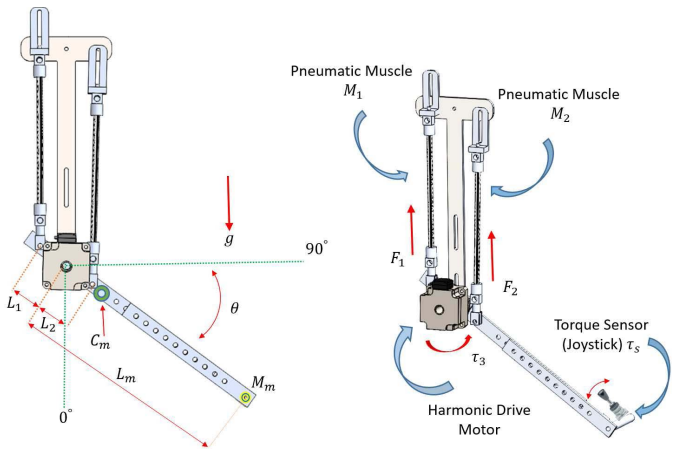

Fig. 2. Free body diagram of the exoskeleton elbow joint.

the parts belonging to the forearm, the arm, and the shoulder. The data obtained from this stress analysis are presented in Table I. We can conclude that the chosen material is adequate and safe for the efforts generated in the exoskeleton.

B. Instrumentation

The exoskeleton has two pneumatic muscles, which are placed in an antagonist position, and they are parallel to the biceps and triceps muscles of the human arm. The pneumatic muscles give the exoskeleton the necessary force to flex and to extend the user arms and to carry heavy objects. The proposed exoskeleton has also parallel Harmonic Drive electrical motors placed in parallel to each elbow joint, which contribute to the system with a percentage of torque, but they also give the precision to get softly desired positions, with a minimum angular position error. The motor shaft coincides with the rotation axis of the antagonist muscle of the system, both actuators must work synchronized, and in this sense, the exoskeleton is hybrid. For the autonomy of the exoskeleton, 24-V batteries are used to energize the electrical motors and two tanks of compressed air, which store 4 L to 10 bars of pressure for the pneumatic muscles.

The exoskeleton is controlled and monitored by an embedded device (NI myRIO-1900) from the National Instruments. It has an ARM Cortex-A9 dual-core processor, and the card has inputs and outputs with MXP and SMP connections. This low-cost PAC is programed by data flow in the LabVIEW software and the controllers are implemented on the PAC. An incremental encoder 6B2-CWZ3E to obtain the angular position is placed on the rotation axis. The prototype contains an air pressure sensor in each pneumatic muscle.

The exoskeleton is commanded by a joystick that is the human force sensor. The joystick is placed at the end of the exoskeleton arm at the height of the user hand (see Fig. 2). When the user is wearing the exoskeleton and flexes the elbow, he can push the joystick with user hand in the direction of the flexion, using only the force necessary to move the joystick. With this intuitive movement, the human flexes the elbow of the exoskeleton to the desired position. The exoskeleton may be carrying a weight, but the torque that is needed to turn the elbow is generated by the exoskeleton's actuators so that the human does not exert more effort. In the same way, when the human extends his elbow can push with his hand the joystick in the direction of the extension by intuitively moving the arm of the exoskeleton in the desired direction. The speed and direction of rotation in the articulation of the exoskeleton are proportional to the force exerted on the joystick. In this sense, the joystick works like a torque sensor, considering Hook's law as

$$\tau_s = (\theta_s - \theta_s(0))k_s \tag{1}$$

where τ_s is the exerted torque in the joystick, θ_s is the rotation angle and $\theta_s(0)$ is the angle on the equilibrium position, and k_s is the elasticity coefficient. Intuitively, when the user exerts a small torque on the sensor of around 13 Nm, an amplified torque is generated by the exoskeleton.

III. Mathematical Model

In this section, the mathematical model of the proposed exoskeleton is presented. The continuous nonlinear model is presented, and then, its discrete version is obtained.

A. Continuous Model

Although a human elbow joint can rotate 150°, the exoskeleton is designed to rotate only 70° with an initial position at 20° and final position at 90°.

The reason for this restriction arises because the main objective is to lift objects. Therefore, when the arms are maintained at 90°, the load is lifted safely, while the shoulder joint remains static [24].

The mathematical model was obtained from the free body diagram of the exoskeleton shown in Fig. 2, where g is gravitational constant, M_p is the load mass, τ_3 is the torque of a Harmonic Drive motor, F_1 is the linear force exerted by the pneumatic muscle M_1, F_2 is the linear force exerted by the pneumatic muscle M_2, L_1 is the distance from the pivot to the muscle M_1, L_2 is the distance from the pivot to the muscle M_2, and L_m is the distance from the pivot to the loading point.

The pneumatic muscles are antagonistic. When the pneumatic muscle M_1 is inflated, it generates a torque in the anticlockwise direction of the joint, while the pneumatic muscle M_2 simply deflates and does not exert any torque on the joint. In the same way, when M_2 is inflated, it generates a clockwise torque and M_1 does not exert any torque on the joint. To interpret this, the $\omega(z)$ function was defined as

$$\omega(z) := \begin{cases} 1, & \text{if } z \geq 0 \\ 0, & \text{if } z < 0. \end{cases} \tag{2}$$

The dynamical model was obtained using the Newton–Euler approach and combined with $\omega(z)$ as

$$\begin{aligned}[I_{\text{cm}} + ml^2]\ddot{\theta} = {} & F_1\omega(\theta - \theta_0)L_1 \sin\theta \\ & - F_2\omega(\theta_0 - \theta)L_2 \sin\theta \\ & + \tau_3 + M_p g L_m \text{sen}\theta - b\dot{\theta} \end{aligned} \tag{3}$$

where m is the forearm mass, l is the distance from the pivot to the mass center of the forearm, b is the friction constant in the joint, I_{cm} is the moment of inertia of the forearm with

This article has been accepted for inclusion in a future issue of this journal. Content is final as presented, with the exception of pagination.

respect to axis that passes through their mass center C_m, θ is the angular position, and θ_0 is the angular position of the forearm before the moving of the joint. Note that the $\omega(z)$ function of (3) serves to distinguish the active muscle and multiply by 1 the force (F_1 and F_2 belonging to M_1 and M_2) that is generating a torque in the articulation while eliminating the other force that belongs to the inactive muscle, multiplying it by 0.

Define $\theta_1 = \theta$ and $\theta_2 = \dot{\theta_2}$, and then, the state-space representation of the dynamic model is

$$\begin{bmatrix} \dot{\theta_1} \\ \dot{\theta_2} \end{bmatrix} = \begin{bmatrix} \theta_2 \\ \tau_t + \dfrac{M_p g L_m sen\theta_1}{I_{\text{cm}} + ml^2} - \beta\theta_2 \end{bmatrix} \tag{4}$$

where

$$\beta = \frac{b}{I_{\text{cm}} + ml^2} \tag{5}$$

$$\tau_t = \frac{(F_1\omega(\theta - \theta_0)L_1 - F_2\omega(\theta_0 - \theta)L_2)\text{sen}\theta_1 + \tau_3}{I_{\text{cm}} + ml^2}. \tag{6}$$

In Section III-B, the discrete version of this continuous model is presented.

B. Discrete Dynamic Model

First, consider a fixed sample time t_s and $t = kt_s$, where $k = 0, 1, 2, \ldots$ Then, to discretize the dynamic model given by (4), consider that

$$\begin{bmatrix} \theta_1(t) \\ \theta_2(t) \end{bmatrix} \approx \begin{bmatrix} \theta_1(k) \\ \theta_2(k) \end{bmatrix}. \tag{7}$$

The derivative in model (4) is approximated by the Euler approximation as follows:

$$\frac{d}{dt}\begin{bmatrix} \theta_1 \\ \theta_2 \end{bmatrix} \approx \frac{1}{t_s}\begin{bmatrix} \theta_1(k+1) - \theta_1(k) \\ \theta_2(k+1) - \theta_2(k) \end{bmatrix}. \tag{8}$$

Therefore, the discrete dynamic model can be written as

$$\begin{bmatrix} \theta_1(k+1) \\ \theta_2(k+1) \end{bmatrix} = \begin{bmatrix} t_s\theta_2(k) + \theta_1(k) \\ t_s\tau_t(k) + \dfrac{t_s M_p g L_m \sin\theta_1(k)}{I_{\text{cm}} + ml^2} - t_s\beta\theta_2(k) + \theta_2(k) \end{bmatrix}. \tag{9}$$

The last discrete model could be rewritten as the affine nonlinear equation

$$\overline{x}(k+1) = f_0(\overline{x}(k)) + f_1(\overline{x}(k))u(k) \tag{10}$$

where t_s is the sampling time, $\overline{x}(k) = [\theta_1 \ \ \theta_2]^T$, $k = 0, 1 \ldots$,

$$f_0(\overline{x}(k)) = \begin{bmatrix} \theta_1(k) + t_s\theta_2(k) \\ \theta_2(k)\,(1 - t_s\beta) + \dfrac{t_s M_p g L_m \sin(\theta_1(k))}{I_{\text{cm}} + ml^2} \end{bmatrix} \tag{11}$$

$$f_1(\overline{x}(k)) = \begin{bmatrix} 0 & 0 & 0 \\ \dfrac{L_1 \sin\theta_1(k)}{c_1} & \dfrac{-L_2 \sin\theta_1(k)}{c_1} & \dfrac{1}{c_1} \end{bmatrix} \tag{12}$$

with $c_1 = I_{\text{cm}} + ml^2$, and

$$u = \begin{bmatrix} F_1\omega(\theta_1 - \theta_0) \\ F_2\omega(\theta_0 - \theta_1) \\ \tau_3 \end{bmatrix}. \tag{13}$$

In Section IV, a procedure that minimizes a quadratic index performance in the local sense is presented. The algorithm is based on the DP, which is originally exposed in [25] and [26] and used in a quadrotor in [27]; however, to the best of our knowledge, this discrete control based on the classical DP has not been used in exoskeletons.

IV. Optimization Procedure of Finite Horizon

The task development of the proposed exoskeleton is defined in a finite period of time and the energy used by the three actuators is computed by the control algorithm. This is a crucial issue since the minimization of the energy spent in the control system will directly affect the time autonomy of the prototype. This motivates the use of a discrete DP approach to find an optimized control sequence for finite horizon and is described next.

A. Suboptimal Discrete Control Sequence

Consider the following definition of the controllability of a pair point.

Definition 1: The pair (x_0, x_1) is controllable, if there exists an admissible control $u(k)$ such that the system defined by $x(k+1) = f(x(k), u(k))$ is transferred from x_0 to x_1 in N finite number of steps, where $f(x(k), u(k)) \in R^n$, $u(k) \in R^m$.

It is not a hard task to verify that the systems (10)–(13) are locally controllable around to the fixed-point zero.

Now, consider the quadratic performance index defined in [26] as

$$J = \frac{1}{2}\bar{x}^T(N)H\bar{x}(N) + \frac{1}{2}\sum_{k=0}^{N-1}\{\bar{x}^T(k)Q\bar{x}(k) + u^T(k)Ru(k)\} \tag{14}$$

with the horizon as $t_f = t_s N$, t_s is the sample period, and $N \in \mathbf{N}$. The Q and R are square positive-semidefinite and positive-definite matrices, respectively. Assume that the pair of points (x_0, x_{tf}) of the system (10)–(13) satisfy *Definition 1*. The DP approach in discrete time proposed in [26] is used to obtain

$$J^*_{N,N} = \frac{1}{2}\bar{x}^T(N)H\bar{x}(N). \tag{15}$$

This term does not depend on the control law $u(N)$, because $\bar{x}_N$ depends on the control u_{N-1}; then, one can conclude that $J^*_{N,N}$ is the optimal value of J in the discrete time N and then $u^*(N) = 0$. Then, in the next step, we want to optimize the performance index J with respect to the control u_{N-1} as follows:

$$J^*_{N-1,N} = \min_{u(N-1)}\left\{J^*_{N,N} + \frac{1}{2}\bar{x}^T(N-1)Q\bar{x}(N-1) + \frac{1}{2}u^T(N-1)Ru(N-1)\right\}. \tag{16}$$

This article has been accepted for inclusion in a future issue of this journal. Content is final as presented, with the exception of pagination.

As $\bar{x}(N-1)$ depends of the control $u(N-2)$, we only consider the state $\bar{x}(N)$ from (10), and then

$$\begin{aligned} J^*_{N-1,N}(\bar{x}(N-1),u(N-1)) &= \min_{u(N-1)} \left\{ \frac{1}{2}[f_0(\bar{x}(N-1)) + f_1(\bar{x}(N-1)u(N-1)]^T \right. \\ &\quad \times H[f_0(\bar{x}(N-1)) + f_1(\bar{x}(N-1)u(N-1))] \\ &\quad + \frac{1}{2}\bar{x}^T(N-1)Q\bar{x}(N-1) \\ &\quad \left. + \frac{1}{2}u^T(N-1)Ru(N-1) \right\}. \end{aligned} \tag{17}$$

To find a local minimal value of $J_{N-1,N}$ with respect to $u(N-1)$, first, consider that the existence of a minimum is guaranteed, because the right-hand side of (17) is strongly convex with respect to $u(N-1)$, and then, by using the sufficient condition of the fundamental theorem of the variational calculus [26]

$$\frac{\partial J_{N-1,N}}{\partial u(N-1)} = 0 \tag{18}$$

it follows that:

$$\begin{aligned} u^*(N-1) = -[f_1^T(\bar{x}(N-1))Hf_1(\bar{x}(N-1)) + R]^{-1} \\ \times f_1^T(\bar{x}(N-1))Hf_0(\bar{x}(N-1)). \end{aligned} \tag{19}$$

The term $[f_1^T(\bar{x}(N-1))Hf_1(\bar{x}(n-1)) + R]^{-1}$ exists, because $R > 0$. Observe that the control given by (19) is optimal, because

$$\frac{\partial^2 J_{N-1,N}(\bar{x}(N-1),u(N-1)}{\partial^2 u(N-1)} = R > 0. \tag{20}$$

For the next step $N-2$, note that the value of $u^*(N-1)$ is the optimal value in the step $N-1$, and according to the Bellman optimality principle, this control generates the optimal value for $\bar{x}(N-1)$. Then, we have that

$$\begin{aligned} \bar{J}_{N-2,N}(\bar{x}(N-2),u(N-1),u(N-2)) &= \min_{u(N-1)\ ,u(N-2)} \left\{ \frac{1}{2}\bar{x}(N)^T H\bar{x}(N) + \cdots + \frac{1}{2}\bar{x}^T(N-1) \right. \\ &\quad \times\ Q\bar{x}^T(N-1) + \frac{1}{2}\bar{x}^T(N-2)Q\bar{x}(N-2) \\ &\quad +\ \frac{1}{2}u^T(N-1)Ru(N-1) \\ &\quad \left. + \frac{1}{2}u^T(N-2)Ru(N-2) \right\}. \end{aligned} \tag{21}$$

The term including $\bar{x}(N)$ depends on the control $u(N-1)$ and the term including $\bar{x}(N-2)$ depends on the control $u(N-3)$, and then, only the term with $\bar{x}(N-1)$ depends on the control $u(N-2)$. As the control $u(N-1)$ in the previous step is optimal, the minimization is made only with respect to $u(N-2)$ and $\bar{x}(N-1)$ is obtained by the state equation (10), and it follows that:

$$\begin{aligned} \bar{J}_{N-2,N}(\bar{x}(N-2),u(N-2)) &= \min_{u(N-2)} \left\{ \frac{1}{2}\bar{x}(N)^T H(\bar{x})(N) + \frac{1}{2}[f_0(\bar{x}(N-2)) \right. \\ &\quad + \cdots + f_1(\bar{x}(N-2))u(N-2)]^T \\ &\quad \times\ Q[f_0(\bar{x}(N-2)) + f_1(\bar{x}(N-2))u(N-2)] \\ &\quad +\ \frac{1}{2}\bar{x}^T(N-2)Q\bar{x}(N-2) \\ &\quad +\ \frac{1}{2}u^T(N-1)Ru(N-1) \\ &\quad \left. + \frac{1}{2}u^T(N-2)Ru(N-2) \right\}. \end{aligned} \tag{22}$$

We use the last equation to obtain the suboptimal control $u(N-2)$, without solving the Riccati equations, which is a very complex problem. However, (21) is strongly convex with respect to $u(N-2)$, and this fact guarantees the existence of a minimum; however, it is only an approximation of the optimal value of $u(N-2)$, since, as it is well known, the optimal control signal $u(N-2)$ should be found applying the solution of the Riccati equation. We proceed in the usual manner in order to find the suboptimal control $u(N-2)$ $(\partial J_{N-2,N}/\partial u(N-2) = 0)$

$$\begin{aligned} \bar{u}(N-2) = -\left[f_1^T(\bar{x}(N-2))Qf_1(\bar{x}(N-1)) + R\right]^{-1} \\ \times f_1^T(\bar{x}(N-1))Qf_0(\bar{x}(N-1)). \end{aligned} \tag{23}$$

The general equations are obtained as follows:

$$\begin{aligned} \bar{u}(N-k) = -\left[f_1^T(\bar{x}(N-k))Qf_1(\bar{x}(N-k)) + R\right]^{-1} \\ \times f_1^T(\bar{x}(N-k))Qf_0(\bar{x}(N-k)) \end{aligned} \tag{24}$$

and

$$\begin{aligned} \bar{J}_{N-k,N}(\bar{x}(N-k),u(N-k)) &= \bar{J}_{N-k+1,N} + \frac{1}{2}\bar{x}^T(N-k)Q\bar{x}(N-k) \\ &\quad + \bar{u}^T(N-k)R\bar{x}(N-k) \end{aligned} \tag{25}$$

for all $k = 2, \ldots, N$, for $k = 1$, the control is given by (19).

This suboptimal sequence obtained here guarantees that an approximation to the minimal value to the performance index (14) is reached.

Remark 1: From (25), note that $\bar{J}_{N-k,N} > \bar{J}_{N-k+1,N}$, then $\bar{J}_{.,.}$ is a decreasing function and it is a quadratic function; it implies that the state tends to fixed point.

B. Suboptimal Control for the Exoskeleton

The suboptimal control sequence previously described is used to control the position and velocity of the exoskeleton. Although the expressions presented here are referenced to the fixed-point zero, in the real-time implementation, the error is used instead of only the state.

Consider the discrete mathematical model (10)–(13), the quadratic performance index (14), the suboptimal sequence (24), and the following penalty matrices in the

This article has been accepted for inclusion in a future issue of this journal. Content is final as presented, with the exception of pagination.

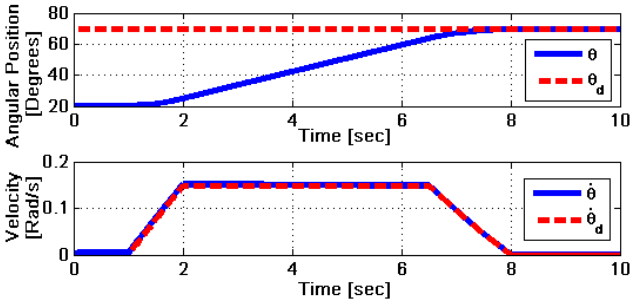

Fig. 3. Position control simulation with the suboptimal control law applied to the exoskeleton mathematical model with a predefined velocity profile.

criterion (14)

$$R = \begin{bmatrix} R_{11} & 0 & 0 \\ 0 & R_{22} & 0 \\ 0 & 0 & R_{33} \end{bmatrix}$$

and

$$H = Q = \begin{bmatrix} Q_{11} & 0 \\ 0 & Q_{22} \end{bmatrix}.$$

For these chosen matrices, the control signal (24) is

$$u = \begin{bmatrix} u_1 \\ u_2 \\ u_3 \end{bmatrix} = \begin{bmatrix} -2CL_1R_{22}R_{33}t_s \dfrac{\sin B}{E}G \\ 2DL_2R_{11}R_{33}t_s \dfrac{\sin B}{E}G \\ -2R_{11}R_{22}\dfrac{t_s}{E}G \end{bmatrix} \tag{26}$$

where u_1 is the suboptimal control law corresponding to the first pneumatic muscle, which produces the force F_1, u_2 is the suboptimal control law corresponding to the second muscle associated with the force F_2, and u_3 is the suboptimal control corresponding to the Harmonic Drive motor, $B := \theta_1(k)$, $A := \theta_2(k)$, $C := \omega(\theta_1(k)) - \theta_1(0)$, $D := \omega(\theta_1(0) - \theta_1(k))$ and

$$\begin{aligned} E =\ & 2R_{11}R_{22}R_{33}I_{\text{cm}}^2 + 2Q_{22}R_{11}R_{22}t_s^2 \\ & + 2m^2l^4R_{11}R_{22}R_{33} + D^2L_2^2Q_{22}R_{11}R_{33}t_s^2 \\ & + 4ml^2R_{11}R_{22}R_{33}I_{\text{cm}}C^2L_1^2Q_{22}R_{22}R_{33}t_s^2 \\ & + C^2L_1^2Q_{22}R_{22}R_{33}t_s^2 \sin 2B \\ & + D^2L_2^2Q_{22}R_{11}R_{33}t_s^2 \sin 2B \end{aligned} \tag{27}$$

and

$$\begin{aligned} G =\ & AQ_{22}I_{\text{cm}} - AbQ_{22}t_s + Amr^2Q_{22} \\ & + M_pgL_mQ_{22}t_s \sin B. \end{aligned} \tag{28}$$

The specific choice of the diagonal penalty matrices gives a particular structure of the controller. Note that the controller involves position and velocity.

V. Results

In this section, simulation and experimental results are presented. Furthermore, the suboptimal control proposed in this brief is compared with a proportional and derivative control with gravity compensation (PD + G) to highlight some advantages concerning the closed-loop performance. In addition, the control PD + g is considered a suitable control for this type of exoskeletons focused on assisting the user in the load of heavy objects, since the nature of the control is to compensate the torque necessary to hold an object in an angular position.

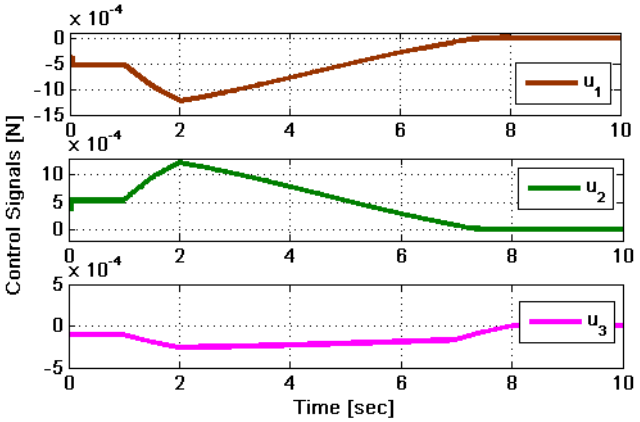

Fig. 4. Simulated control signals u_1 and u_2 for the pneumatic muscles M_1, M_2 and control u_3 for the harmonic drive motor.

A. Numerical Results

The first test of the exoskeleton mathematical model is a stabilization task. The objective is to reach an angular position of 70° and to maintain it for 5 s and then come back to the initial angular position of 20°, following the previously established velocity profile.

The simulation results are shown in Fig. 3, when the position and the angular velocity are displayed. The simulation parameters are $M_p = 5$ kg, $L_m = 0.35$ m, $I_{\text{cm}} = 0.0469$ kgm^2, $m = 200$ g, $r = 0.18$ m, $b = 0.010$, $t_s = 0.05$ s,$L_1 = 0.0532$ m, $L_2 = 0.0532$ m, $R = [100; 010; 001]$, and $Q = H = [10\,0;\ 0\,15]$

Fig. 4 shows the control signals in simulation u_1 and u_2 for the pneumatic muscles and the control u_3 corresponding to the harmonic drive motor.

A suboptimal control for the exoskeleton is proposed with the aim of reducing the pneumatic as well as electrical energy. A comparison of the control signal magnitudes is presented. The total torque τ_t is given by (6). Both the suboptimal control versus the torque produced by a PD + G control are shown in Fig. 5. As can be observed at the beginning of the experiment, the signal given by the PD + G controller has a large energy expenditure. On the other hand, the suboptimal controller signal does not present any peak. We may conclude that the suboptimal control signal stabilizes the plant in a region smaller than the one corresponding to the PD + G controller. The PD + G controller was heuristically tuned and the same control signal was applied to the actuators. Note, however, that it is not an easy task to tune this controller in view of the nonlinearities of the plant. In the case of the nonlinear suboptimal control, one has to select a pair Q and R. Such a choice is simplified because of the diagonal structure of these matrices.

B. Experimental Results

The suboptimal control laws were implemented in the embedded card MyRIO-National Instruments with a sampling

This article has been accepted for inclusion in a future issue of this journal. Content is final as presented, with the exception of pagination.

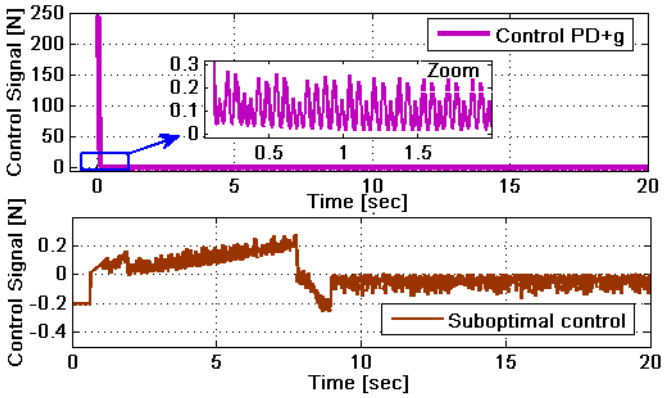

Fig. 5. Simulation results of a comparison of control signals magnitude between a PD + G controller and a suboptimal control.

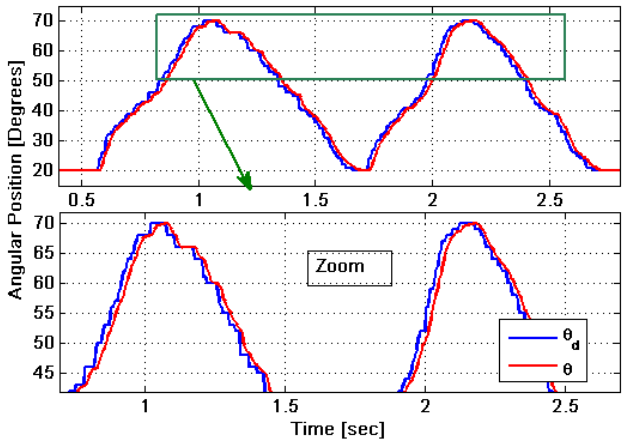

Fig. 6. Real-time experimental results of trajectory tracking generated by a signal obtained by a force sensor when flexes and extends the elbow joint.

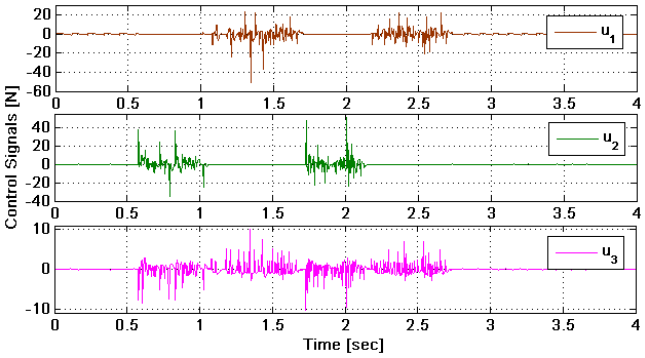

Fig. 7. Real-time control signals (u_1, u_2, and u_3) corresponding to the pneumatic muscles and electric motor for the trajectory-tracking test.

time of 10 ms. The first test consisted in tracking a reference signal that flexes and extends the elbow joint. The reference signal is produced by a joystick manipulated by the user. It is necessary to clarify that the maximum flexion of the prototype occurs at 70° and the minimum at 20°. Fig. 6 shows the experimental results of this task-tracking, and a zoomed-in view on the signal shows that despite the fact that the desired signal has abrupt changes, the real signal is smoother, due to the advantages provided by the actuator dynamics.

The above graph represents the natural movement of the elbow joint during lifting, putting down, and lifting again an

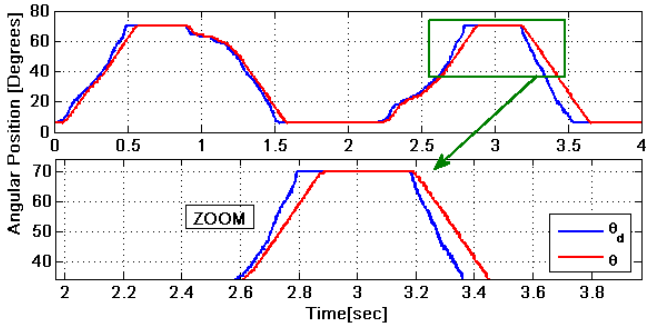

Fig. 8. Real-time experimental results of trajectory tracking when a PD + G control is used.

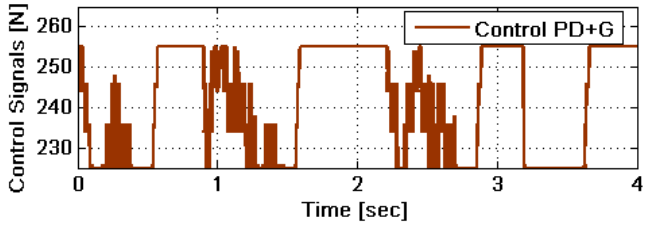

Fig. 9. Real-time control signal of the PD + G control applied to all actuators for the trajectory-tracking test.

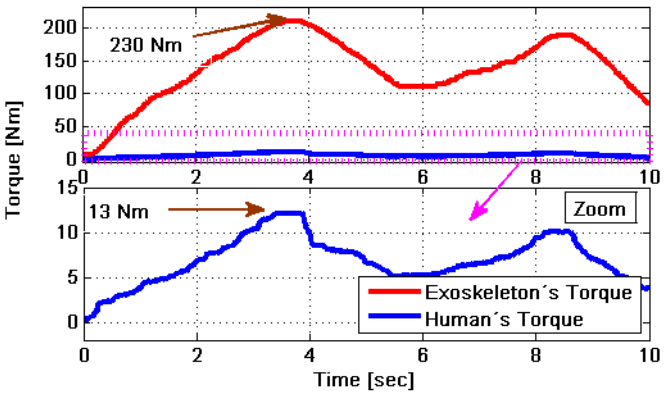

Fig. 10. Comparison of force exerted between the exoskeleton and the human.

object. The control signals corresponding to this experiment are shown in Fig. 7. The antagonist motion of the muscles is due to controls u_1 and u_2. Control u_1 activates to muscle M_2, but this control is also used to control the output airflow of muscle M_1. The same behavior occurs with the control u_2, but in an antagonist way. Control input u_3 is the signal that drives the Harmonic Drive motor.

A similar task was made but using a PD + G control, and the results could be seen in Fig. 8 and the control signal is shown in Fig. 9.

It is clear that the tracking error is greater than the one produced by using the suboptimal discrete nonlinear control, and the signal control of the last controller is smaller in magnitude than the corresponding signal of the PD + G controller.

The good performance of the system, presented in the experimental tests when using the suboptimal control, validates the mathematical model since the design of the suboptimal control is computed using the model. Moreover, in order to evaluate the quality of assistance provided to the user, Fig. 10 shows the

This article has been accepted for inclusion in a future issue of this journal. Content is final as presented, with the exception of pagination.

results comparing the torques generated by the human and by the exoskeleton. Observe that it is necessary for the human to generate a torque not greater than 15 Nm to obtain a torque in the elbow of the exoskeleton of 230 Nm. This rise of strength allows a comfortable behavior.

VI. Conclusion

The mathematical model, the design, the control algorithm, and the prototype of a hybrid exoskeleton were presented. The main contribution is in the configuration of the articulation of the exoskeleton that presents the coupling of two types of actuators by means of a control that optimizes the energy expenditure. The reference for control tracking is generated online with the human intention. This intention is sensed by a joystick placed in the exoskeleton. In the same way, the control (nonlinear suboptimal) makes a satisfactory online tracking.

The proposed nonlinear suboptimal control algorithm for finite horizon was based on the DP approach. Such a control strategy does not require explicit solving of the Bellman equation. Furthermore, the controller parameter tuning is relatively easier than other control algorithms (see Fig. 5) We conclude also that the suboptimal control requires less energy expenditure compared with a classical proportional and derivative control law with gravity compensation. Satisfactory experimental tests were conducted, which verified the feasibility and controllability of the hybrid exoskeleton prototype.

References

[1] J. L. Pons, *Wearable Robots: Biomechatronic Exoskeletons*. Hoboken, NJ, USA: Wiley, 2008.

[2] J. L. A. S. Ramos and M. A. Meggiolaro, "Use of surface electromyography for human amplification using an exoskeleton driven by artificial pneumatic muscles," in *Proc. 5th IEEE RAS/EMBS Int. Conf. Biomed. Robot. Biomechatronics*, Aug. 2014, pp. 585–590.

[3] T. Noda, T. Teramae, B. Ugurlu, and J. Morimoto, "Development of an upper limb exoskeleton powered via pneumatic electric hybrid actuators with bowden cable," in *Proc. IEEE/RSJ Int. Conf. Intell. Robots Syst.*, Sep. 2014, pp. 3573–3578.

[4] A. Pujana-Arrese, A. Mendizabal, J. Arenas, S. Riano, and J. Landaluze, "Research on the position control of a 1-DOF set-up powered by pneumatic muscles," in *Proc. IEEE Int. Conf. Mechatronics*, Apr. 2009, pp. 1–6.

[5] F. Martinez, I. Retolaza, A. Pujana-Arrese, A. Cenitagoya, J. Basurko, and J. Landaluze, "Design of a five actuated DoF upper limb exoskeleton oriented to workplace help," in *Proc. 2nd IEEE RAS EMBS Int. Conf. Biomed. Robot. Biomechatronics*, Oct. 2008, pp. 169–174.

[6] A. Pujana-Arrese, J. Arenas, I. Retolaza, A. Martinez-Esnaola, and J. Landaluze, "Modelling in modelica of a pneumatic muscle: Application to model an experimental set-up," in *Proc. 21st Eur. Conf. Modelling Simulation, ECMS*, Jun. 2007, pp. 4–6.

[7] M. Hamaya, T. Matsubara, T. Noda, T. Teramae, and J. Morimoto, "Learning assistive strategies for exoskeleton robots from user-robot physical interaction," *Pattern Recognit. Lett.*, vol. 99, pp. 67–76, Nov. 2017.

[8] H. Seo and S. Lee, "Design and experiments of an upper-limb exoskeleton robot," in *Proc. 14th Int. Conf. Ubiquitous Robots Ambient Intell. (URAI)*, Jun./Jul. 2017, pp. 807–808.

[9] D. Sui, J. Fan, H. Jin, X. Cai, J. Zhao, and Y. Zhu, "Design of a wearable upper-limb exoskeleton for activities assistance of daily living," in *Proc. IEEE Int. Conf. Adv. Intell. Mechatronics (AIM)*, Jul. 2017, pp. 845–850.

[10] Y. Liu, S. Guo, S. Zhang, and L. Boulardot, "A novel sEMG control-based variable stiffness exoskeleton," in *Proc. IEEE Int. Conf. Mechatronics Autom. (ICMA)*, Aug. 2017, pp. 1444–1449.

[11] S. Crea *et al.*, "A novel shoulder-elbow exoskeleton with series elastic actuators," in *Proc. 6th IEEE Int. Conf. Biomed. Robot. Biomechatronics (BioRob)*, Jun. 2016, pp. 1248–1253.

[12] D. Popov, I. Gaponov, and J.-H. Ryu, "A preliminary study on a twisted strings-based elbow exoskeleton," in *Proc. World Haptics Conf. (WHC)*, Apr. 2013, pp. 479–484.

[13] D. Popov, I. Gaponov, and J.-H. Ryu, "Bidirectional elbow exoskeleton based on twisted-string actuators," in *Proc. IEEE/RSJ Int. Conf. Intell. Robots Syst.*, Nov. 2013, pp. 5853–5858.

[14] S. Guo, J. Gao, J. Guo, and N. Li, "The Lab VIEW-based control system for the upper limb rehabilitation robot," in *Proc. IEEE Int. Conf. Mechatronics Autom. (ICMA)*, Aug. 2017, pp. 1732–1737.

[15] V. Krasin, V. Gandhi, Z. Yang, and M. Karamanoglu, "EMG based elbow joint powered exoskeleton for biceps brachii strength augmentation," in *Proc. Int. Joint Conf. Neural Netw. (IJCNN)*, Jul. 2015, pp. 1–6.

[16] C. A. Cansalar, E. Mavis, and C. Kasnakoglu, "Simulation time analysis of MATLAB/Simulink and LabVIEW for control applications," in *Proc. IEEE Int. Conf. Ind. Technol. (ICIT)*, Mar. 2015, pp. 470–473.

[17] B. Gao, H. Ma, S. Guo, H. Xu, and S. Yang, "Design and evaluation of a 3-degree-of-freedom upper limb rehabilitation exoskeleton robot," in *Proc. IEEE Int. Conf. Mechatronics Autom. (ICMA)*, Aug. 2017, pp. 938–942.

[18] N. Vitiello *et al.*, "NEUROExos: A powered elbow exoskeleton for physical rehabilitation," *IEEE Trans. Robot.*, vol. 29, no. 1, pp. 220–235, Feb. 2013.

[19] M. H. Rahman, T. K-Ouimet, M. Saad, J. P. Kenné, and P. S. Archambault, "Control of a powered exoskeleton for elbow, forearm and wrist joint movements," in *Proc. IEEE Int. Conf. Robot. Biomimetics. IEEE*, Dec. 2011, pp. 1561–1566.

[20] M. Singh and S. Chatterji, "Trends and challenges in emg based control scheme of exoskeleton robots-a review," *Int. J. Sci. Eng. Res.*, vol. 3, no. 8, pp. 933–940, Aug. 2012.

[21] M. R. Tucker *et al.*, "Control strategies for active lower extremity prosthetics and orthotics: A review," *J. Neuroeng. Rehabil.*, vol. 12, no. 1, p. 1, Dec. 2015.

[22] T. Matsubara, T. Noda, S.-H. Hyon, and J. Morimoto, "An optimal control approach for hybrid actuator system," in *Proc. 11th IEEE-RAS Int. Conf. Humanoid Robots*, Oct. 2011, pp. 300–305.

[23] T. Teramae, T. Noda, and J. Morimoto, "Optimal control approach for pneumatic artificial muscle with using pressure-force conversion model," in *Proc. IEEE Int. Conf. Robot. Automat. (ICRA)*, May/Jun. 2014, pp. 4792–4797.

[24] F. Castillo, A. Osorio, R. López, R. Lozano, and O. Santos, "Hybrid, discrete, non-linear, suboptimal force augmenting exoskeleton for the elbow joint," in *Proc. 4th Int. Conf. Control, Mechatronics Automat.*, Dec. 2016, pp. 178–182.

[25] R. Bellman, "Dynamic programming and stochastic control processes," *Inf. control*, vol. 1, no. 3, pp. 228–239, Sep. 1958.

[26] D. E. Kirk, *Optimal Control Theory: An Introduction, Dever Books on Electricarl Engineering Series*. New York, NY, USA: Dover, 2004.

[27] O. García, "RED UAS 2017- research, education and development of unmanned aerial systems," (RED-UAS)," in *Proc. Workshop*, Oct. 2015, pp. 142–151.